Computational Materials Science 149 (2018) 153–157

Contents lists available at ScienceDirect

Computational Materials Science

journal homepage: www.elsevier.com/locate/commatsci

On the performance of interatomic potential models of iron: Comparison of the phase diagrams

Lívia B. Pártay

Department of Chemistry, University of Reading, Reading RG6 6AD, UK

ARTICLE INFO

Keywords:
Nested sampling
Phase diagrams
Phase transition prediction
EAM models for iron

ABSTRACT

In order to study the performance of interatomic potentials and their reliability at higher pressures, the phase diagram of four different embedded-atom type potential models of iron is compared. The calculations were done by the nested sampling technique in the pressure range 0.1–100 GPa. The low pressure stable structure is found to be the body-centred cubic in all cases, but the higher pressure phases show a great variation, being face-centred cubic, hexagonal close-packed and – at very low temperatures – different body-centred tetragonal phases are observed as well. The melting line is overestimated considerably for three of the models, but for the one where liquid properties had been taken into account during the potential fitting process, the agreement with experimental results is good, even at very high pressures.

1. Introduction

When using atomistic simulations, one of the keys to accurately predict the structure and properties of materials and their defects is the quality of the description of atomic interactions. In order to compromise between computational efficiency, generality and accuracy, empirical or semi-empirical potentials are often used as descriptors in most large-scale and long-time computations. These potentials are commonly determined by fitting a proposed functional form to a group of available data, which may be obtained from either experimental measurements or first-principles calculations.

However, it is difficult to predict how these potentials will perform under conditions different from that of the exact fitting parameters. While some of the microscopic properties are likely to be reproduced accurately, the macroscopic behaviour of the potential model can be very different from what is expected, especially the complex phenomena of phase transitions and phase stability. Gaining a better understanding on how the choice of fitting parameters effect the resulting phase diagram can help us not only to determine the reliability of a certain potential model, but to improve strategies of potential development in the future. To be able to do this, it is vital to have a technique which is capable of calculating the entire phase diagram of a potential model in an automated way, without prior knowledge of the phases. In recent years we have been developing such a technique, called nested sampling (NS). NS is a Bayesian statistical method [1,2] we adapted to explore the atomic phase space [3] and has been applied to study clusters and the hard-sphere model [4–6]. In previous papers [7,8] we also showed how the NS algorithm enables the automated calculation of the complete pressure-temperature-composition phase diagram. In the present work I further demonstrate this, using empirical potentials of iron and discussing the emerging differences between the studied models.

1.1. Experimental phase diagram of iron

Iron is one of the most important and widely used technological materials, moreover, it is considered to be the dominant component of the inner core of the Earth. Thus, investigating the properties and phase behaviour of iron is not only of great industrial importance but fundamental in the understanding of geological processes and the inner structure of our planet. However, due to its unique properties, the complex phase diagram of iron is still not fully understood, with details of the melting line and crystal structures at high pressure being in the focus of research for several decades.

At low temperature and pressure iron exists in the α-Fe form, a ferromagnetic bcc structure. With increasing temperature this first transforms to the non-magnetic fcc structure, γ-Fe, then to a ferromagnetic bcc crystal again, called δ-Fe [9]. At higher pressures the hcp structure (ϵ-Fe) becomes stable, the triple point among the bcc, hcp, and fcc structures located at about 11 GPa and 750 K [10]. The ground state structure is predicted to remain hcp up to about 300 GPa, however, the phase diagram and crystal structure properties are well defined only up to 20 GPa. While the transition between the γ-Fe (fcc) and ϵ-Fe (hcp) at temperatures close to the melting is usually seen at approx. 50 GPa [11], some measurements indicate that this happens at significantly higher pressures [12]. First principle calculations predict that

E-mail address: l.bartokpartay@reading.ac.uk.

https://doi.org/10.1016/j.commatsci.2018.03.026
Received 23 January 2018; Received in revised form 12 March 2018; Accepted 13 March 2018

at high temperature and above 300 GPa, the stability of the fcc phase becomes comparable again to that of the hcp, suggesting that at extreme pressures both phases might be stable as well as other close packed stacking sequences [13]. Furthermore, it has been suggested that two more stable crystal structures might exist: there is evidence about the existence of a double-hcp structure, called ϵ'-Fe between 15 GPa and 40 GPa [14], and speculations about a high temperature β-Fe phase (of unknown structure) at pressures above 50 GPa [15,12,16].

The agreement between the melting temperatures measured by different experimental techniques is good up to 20 GPa, though above that there is a discrepancy between the results, with the suggested melting temperature ranging from 2800 K to 4100 K at 100 GPa [17–20,15,12,21].

1.2. Potential models for iron

In order to gain a better understanding on the properties of iron, different computer simulation and modelling techniques are regularly used to study e.g. the crystal stability, surface properties, defects or radiation damage. Several interatomic potential models have been developed in the past decades to allow large scale calculations, especially within the embedded atom model (EAM) framework [22–27].

One of the most widely used EAM potentials for iron was developed by Ackland et al. [24]. The coefficients of this potential were chosen to fit the lattice parameter, cohesive energy, unrelaxed vacancy formation energy and elastic constants for α-Fe at $T = 0$ K. I will refer to this potential as *Ackland97*. This potential is known to overestimate the melting point by at least 500 K at ambient pressure and provides a liquid structure that is more ordered than observed experimentally [25].

A set of potentials were developed by Mendelev et al. [25] with liquid parameters taken into account during the fitting procedure. As a result these EAM models reproduce well the melting data and liquid structure factor of iron. I chose the recommended potential Nr.2 to use in the current study and will refer to this potential as *Mendelev03*.

Chamati et al. published a model [26], where both DFT and experimental data were included in the parameter fit (elastic constant, vacancy formation), including the energies of bcc, fcc, simple cubic and diamond cubic structures. The potential accurately predicts bulk and surface properties for both bcc and fcc iron, as well as describing the surface migration, phonon dispersion curves and thermal expansion properties, though these were not included while fitting the potential parameters. I will refer to this potential as *Chamati06*.

Another EAM potential was developed by Marinica et al., where although liquid properties were not included in the fit, DFT defect formation and migration energies were [27,28]. I will refer to this potential as *Marinica07*.

It has to be noted that these EAM models lack the description of magnetic properties which play a significant role in solid-solid transitions [29,30], moreover, due to the general formalism of the EAM potential, the interactions are spherically symmetric, missing the effect of directionality caused by the partially filled d bands of iron. More complex interaction models are capable of providing a more accurate description of phase behaviour, such as MEAM [23], bond-order potentials which can predict the bcc-hcp phase transition correctly [31] and the transition sequence of α–γ –δ phases [32], or magnetic bond-order potentials, which reproduces accurately the relative stability of different magnetic bulk phases [33]. Nevertheless, due to their relative simplicity and low computational cost, EAM potentials are extensively used for studying different properties of iron, thus understanding the phase behaviour of these models is an important information for a wide range of applications.

2. Computational details

The nested sampling calculations were performed as presented in [7]. The simulations were run at constant pressure, and the simulation cell of variable shape and size contained 64 atoms. The initial configurations were generated randomly. New samples were generated with performing Hamiltonian Monte Carlo [8] (all-atom) moves, and changing the volume and the shape of the cell by shear and stretch moves. Overall 800 steps were performed at every iteration with ratio 1:2:2:2, respectively. Parallel implementations of this algorithm is available in the `pymatnest` python software package [34], using the LAMMPS package [35] for the dynamics.

Table 1
Typical number of walkers and the associated computational cost. Total force evaluations are counted as for 64 atoms.

Number of walkers	Total force evaluations	CPU (h)
640	9.6×10^8	640
1280	1.9×10^9	1280
1920	3.8×10^9	3460
4800	8.6×10^9	8820

The number of walkers were chosen such that the difference in the melting temperature predicted by independent parallel runs is less than 100 K, and the solid-solid transition is reliably found. At pressures where there are no solid-solid transition, 640 or 1280 walkers were enough to reach convergence, and when solid-solid transition were present 1920 walkers were needed. The exception is the high pressure hcp-fcc transition of the Chamati06 potential, where 4800 walkers were needed to consistently see the transition. The computational cost associated with different number of walkers is shown in Table 1. The error bars reported on the phase diagrams correspond to the full width at half maximum of the heat capacity peaks.

When the sampling process was finished, the heat capacity curves were calculated, its peak positions allowing us to draw the phase diagram. To aid the identification of the solid structure and determine the solid-solid phase transitions both the bond order parameters [36] and the weighted average of radial distribution functions were used.

3. Results

3.1. Potential Ackland97

Heat capacity curves and the phase diagram of the Ackland97 potential are shown in Figs. 1 and 2, respectively. The melting line is overestimated considerably, with the low pressure melting point being about 700 K higher than the experimental value, with the same trend continuing at higher pressures. The only stable solid structure is bcc in the studied pressure range, but the fcc phase, which is metastable for this model, has also been studied [37].

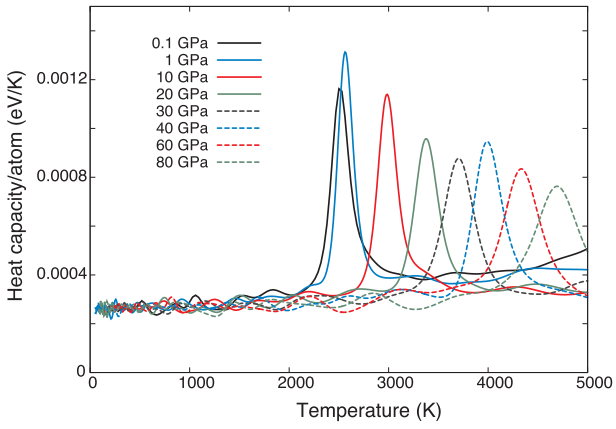

Fig. 1. Heat capacity curves of the Ackland97 potential at different pressures. The peaks correspond to the melting transition.